Photothermal Absorption Correlation Spectroscopy

Vivien Octeau,[†] Laurent Cognet,[†] Laurence Duchesne,[‡] David Lasne,[†] Nicolas Schaeffer,[‡] David G. Fernig,[‡] and Brahim Lounis[†,*]

[†]Centre de Physique Moléculaire Optique et Hertzienne, Université de Bordeaux and CNRS, 351 cours de la Libération, Talence, F-33405, France, and [‡]Centre for Nanoscale Science, School of Biological Sciences, Department of Chemistry, University of Liverpool, Liverpool, L69 7ZB, U.K.

ABSTRACT Fluorescence correlation spectroscopy (FCS) is a popular technique, complementary to cell imaging for the investigation of dynamic processes in living cells. Based on fluorescence, this single molecule method suffers from artifacts originating from the poor fluorophore photophysics: photobleaching, blinking, and saturation. To circumvent these limitations we present here a new correlation method called photothermal absorption correlation spectroscopy (PhACS) which relies on the absorption properties of tiny nano-objects. PhACS is based on the photothermal heterodyne detection technique and measures akin FCS, the time correlation function of the detected signals. Application of this technique to the precise determination of the hydrodynamic sizes of different functionalized gold nanoparticles are presented, highlighting the potential of this method.

KEYWORDS: photothermal detection · correlation spectroscopy · single molecule · gold nanoparticles

In the growing field of nanoscience, detection and characterization tools are essential. The most sensitive methods allow the precise detection of individual nano-objects. Among them, fluorescence-based optical methods are extremely versatile and therefore widely applied. For instance, fluorescence correlation spectroscopy (FCS) is a powerful technique for the study of small numbers of luminescent nano-objects. Following its introduction,[1−4] FCS and its derivate techniques have been essential for the investigation of fluorescent molecule photophysics, diffusion, reaction kinetics as well as for biological studies of molecular dynamics in live cells.[5−9] However, the dynamic range accessible by FCS is limited by nonideal fluorophore photophysics on short time scales and photobleaching for long ones. Furthermore, one of the most significant and often overlooked factors is optical saturation which also influences FCS measurements.[10]

An elegant alternative to FCS would rely on absorption of nanolabels which display favorable photophysics and unlimited photostability. For instance, gold nanoparticles (NPs) are broadly used for applications in nanotechnology and biotechnology due to their optical, chemical, and biocompatible properties.[11,12] They are commonly detected *via* Rayleigh scattering thanks to their optical resonances in the visible range.[13] Accordingly, dynamic light scattering (DLS) is a common method for size measurements of nanometers-scale scatterers in bulk samples.[14,15] However, DLS measurements are limited to environments that are free from background scattering and require rather extensive time averaging.

Recently developed far-field optical techniques based on the detection of a wave scattered either by nanoparticles themselves or by their close environment, allow studies of tiny metal NPs at the single particle level.[16−21] The most sensitive of these methods probes the NPs absorption though the photothermal effect[17] and was applied for the detection and spectroscopy of immobilized NPs as well as for tracking membrane proteins moving at the surface of living cells for arbitrary long times.[22]

Here, we introduce a new correlation method for the study of the diffusion properties of tiny absorbing NPs (down to 5 nm for gold). Analogous to FCS, it measures the time correlation function of the NPs photothermal signal which is directly proportional to the light absorption by the nano-objects and is thus named photothermal absorption correlation spectroscopy (PhACS). Since absorption by a metal NP neither saturates nor photobleaches at reasonable excitation intensities, or contains complicated photophysics, PhACS is free from the majority of the limitations encountered by FCS. Furthermore, as the signals arise from

*Address correspondence to b.lounis@cpmoh.u-bordeaux1.fr.

Received for review November 14, 2008 and accepted January 24, 2009.

Published online February 3, 2009.
10.1021/nn800771m CCC: $40.75

the photothermal effect, the scattering background problem of DLS is also circumvented. Highlighting the potential of PhACS, we then present application of this technique to the precise determinations of the hydrodynamic size of different protein-NP complexes.

RESULTS AND DISCUSSION

Principles of PhACS. PhACS relies on the photothermal heterodyne detection method which allows the detection of the smallest individual gold nanoparticles in the far optical field. In brief, a time-modulated absorbed beam (~700 kHz) is superimposed with a nonresonant probe beam. When an absorbing nano-object is in the focal volume of the two highly focused beams, the consecutive heating induces a time-modulated variation of the refractive index around this nano-object. The interaction of the probe beam with this index profile produces a scattered field with sidebands at the modulation frequency. The scattered field is then detected in the forward direction through its beatnote with the transmitted probe field which plays the role of a local oscillator akin to a heterodyne technique.[17] In the PhACS scheme the beams and sample positions are kept fixed and the signal fluctuations are recorded at high sampling rate while nanoparticles diffuse in the detection volume (Figure 1(a,b)). Similar to FCS experiments, the PhACS signal consists in the autocorrelation function ($G(\tau)$) of the photothermal signal (S) fluctuations:

$$G(\tau) = \frac{\langle \delta S(t)\, \delta S(t+\tau)\rangle}{\langle S(t)\rangle^2} = \frac{\langle S(t)\, S(t+\tau)\rangle}{\langle S(t)\rangle^2} - 1 \quad (1)$$

where $\langle\ \rangle$ denotes the time average. Assuming a elliptical Gaussian-shaped observation volume and freely diffusing particles, $G(\tau)$ is given by[3]

$$G(\tau) = \frac{1}{N(1+\tau/\tau_D)(1+\tau/(A^2\tau_D))^{1/2}} \quad (2)$$

N is the average number of particles in the observation volume; A is the shape parameter of the observation volume; τ_D is a characteristic diffusion time.

Characterization of the Detection Volume. Accurate knowledge of the detection volume dimensions is crucial to the precise measure of NP diffusion times. Since PhACS uses a combination of two highly focused laser beams the point-spread-function is theoretically given by the product of the two beam profiles,[23] yielding a quasi-confocal Gaussian-shaped detection volume. Because of the high stability of the photothermal signal, the 3D shape of the point-spread-function can be measured accurately by performing a precise 3D scan of immobilized NPs. To achieve this, we performed z-stack image acquisitions of 20 nm diameter gold NPs embedded in a 5% w/w agarose gel sandwiched between two glass slides mounted on a three axis piezoscanning stage (Figure 1b). We determined an elliptical detection volume with a transverse diameter w_{xy} equal to 310 ± 3 nm and a shape parameter S of (quotient of axial and lateral diameter $A = w_z/w_{xy}$) equal to 8.4 ± 1.0.

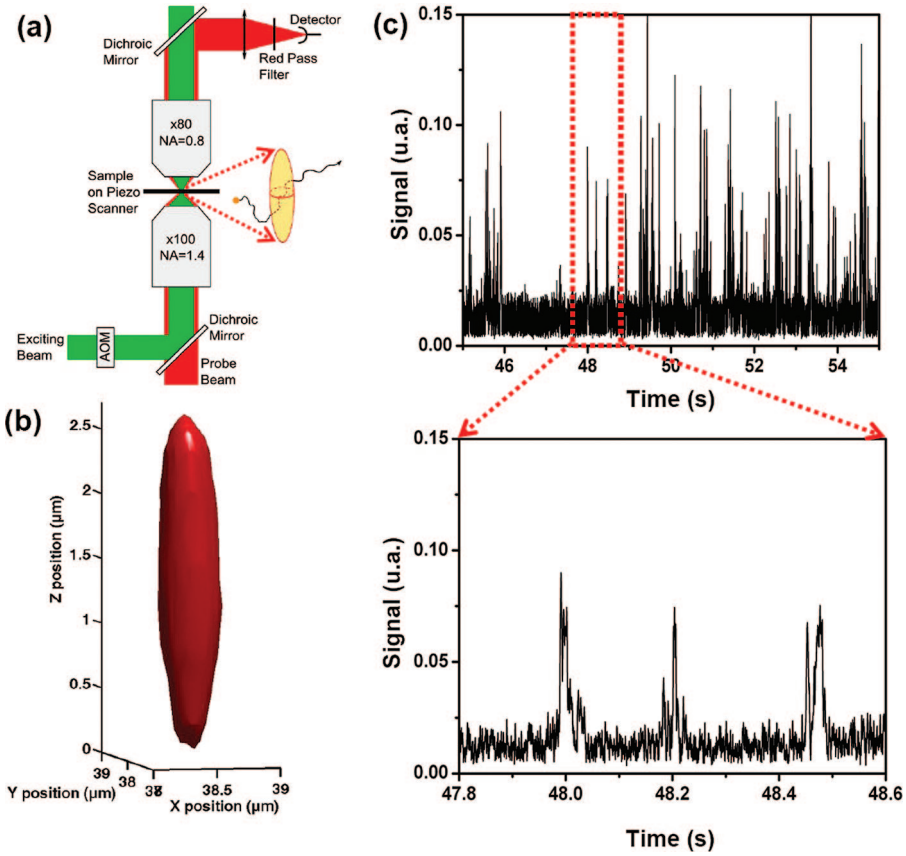

Figure 1. (a) PhACS setup; (b) 3D detection volume measured by z-stack images of a single 20 nm gold NP immobilized in agarose gel; (c) time trace obtained from 10 nm gold NPs in 80% glycerine solutions. Inset: individual NPs passing in the detection volume.

Brownian Motion of Gold Nanoparticles in Solution: Benefits of PhACS. We first studied gold NPs with diameters of 5, 10, or 20 nm freely diffusing in different water/glycerin solutions (0%, 60%, 80%, 95% glycerin w/w). In such isotropic media, the diffusion coefficient D is well-known and relates the NP hydrodynamic diameter d and the fluid viscosity η by the Stokes−Einstein relation: $D = (k_BT)/(3\pi\eta d)$ where k_B is the Boltzmann constant and T is the temperature. Using PhACS measurements (similar to FCS experiments), the measured diffusion time is linked to D through

the relation[3] $4D\tau_D = w_{xy}^2$. The NPs diffusion time can thus be expressed as a function of the medium viscosity and the NPs hydrodynamic diameter by:

$$\tau_D = \gamma\eta d \qquad (3)$$

where γ is a parameter only depending on the temperature and on the setup geometry: $\gamma = (3\pi w_{xy}^2)/(4k_BT)$.

Examples of normalized PhACS curves obtained for NPs diffusing in different medium viscosities are displayed in Figure 2. Each curve was fitted before normalization according to eq 2 with two free parameters (N and τ_D) and one known parameter (A). N ranged typically from 0.01 to 0.3. The typical dispersion in size (and thus diffusion times) of the gold NPs used here was ~10% (determined by electron microscopy) and has a minimal influence on the correlation decay functions as illustrated by the quality of the fits using eq 2 and consistent with previous FCS theoretical and experimental work.[24] Figure 3 displays the measured evolution of τ_D and the corresponding diffusion constant for all products ηd studied (eq 3). The expected linear relationship is obtained on more than three decades. More quantitatively, we found an experimental value of $\gamma_{exp} = 0.54 \pm 0.02 \times 10^8$ m$^2 \cdot$ J^{-1} from the linear fit in agreement the theoretical value of $\gamma_{th} = 0.55 \times 10^8$ m$^2 \cdot$ J^{-1} illustrating the possibility to measure absolute hydrodynamic diameters of absorbing nano-objects with PhACS.

These curves show that PhACS provides a way to measure and quantify the diffusion of absorbing NPs of different sizes in environments with various viscosities. Diffusion time scales and their corresponding diffusion constants covered a wide range (seconds to submilliseconds to corresponding to $D \approx 0.01-100$ μm^2/s) which should find many applications in biology where diffusion constants of biomolecules are extremely diverse. Noteworthy, PhACS correlation times arise exclusively from the diffusive properties of the nanoparticles (Figure 2). On the other hand, the interpretations

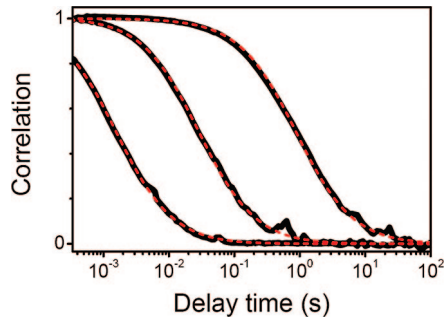

Figure 2. Examples of normalized PhACS curves obtained from different samples measured at 293 K: 5 nm gold NPs in 30% glycerin (left), 10 nm gold NPs in 80% glycerin (middle), and 20 nm gold NPs in 97% glycerin (right). Red dashed lines represent theoretical fits using eq 2.

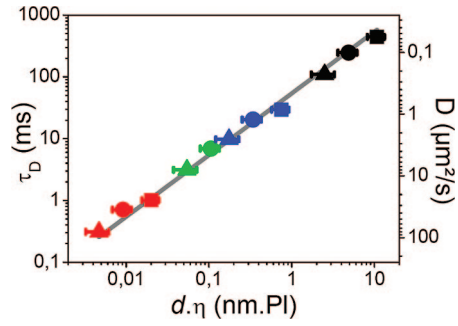

Figure 3. Characteristic diffusion time τ_D for 5 nm (▲), 10 nm (●), and 20 nm (■) nanoparticles in different samples: pure water (red); 60% glycerin (green); 80% glycerin (blue); 95% glycerin (black). The solid line represents a linear fit of τ_D as a function of ηd.

of FCS autocorrelation function are complicated by the photophysical properties of the dyes.[25] On short time scales, while FCS is influenced by the triplet state relaxations which might interfere with fast dynamics,[26,27] PhACS is ultimately limited by the modulation frequency of the exciting beam which can be increased to probe fast dynamics. Note that the decrease of photothermal signal with the modulation frequency[17,23] can be compensated for by the use of larger gold nanoparticles (as the signal scales as $\propto d^3$) or greater excitation powers. On the longer time scales, PhACS is not limited by photobleaching or blinking, and allows exploring extremely slow dynamics. The stability of the photothermal signals also allows an accurate and simple determination of the detection volume and thus precise derivation of the hydrodynamic diameter from the diffusion times. Finally the photothermal signal does not saturate at the standard intensities used (few hundreds of kW/cm^2) because of the fast relaxation times of the NP after excitation (electron−electron and electron−phonon relaxation times remain below 1 ps[28]), whereas FCS experiments should in principle be performed in the zero excitation intensities limit to avoid artifacts due to the saturation of the fluorescent dyes.[27,29]

Hydrodynamic Diameter of Nanoparticles-Protein Complexes. For many applications precise knowledge of the hydrodynamic diameter of functionalized NPs (and their level of aggregation) at low concentration in small volumes is desirable, for example, the hydrodynamic sizes of NP-ligand complexes is of great importance for the study of the protein diffusion in confined areas.[30] Along this line, we show that fast and accurate determinations of the hydrodynamic size of different gold NP complexes at nM concentrations are possible with PhACS. First, we used two reference samples containing bare gold colloid in water (mean diameters of 4.8 and 9.2 nm as determined by electron microscopy) to accurately link the PhACS diffusion times τ_D, with the hydrodynamic diameter of the particles d and avoid the need of a precise

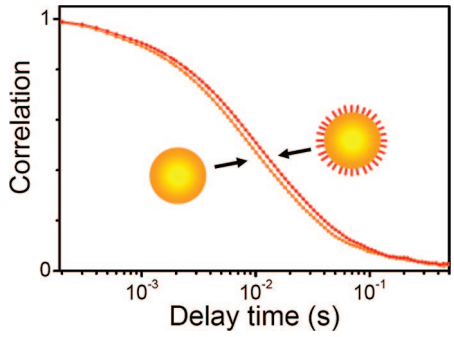

Figure 4. PhACS curves from bare and CALNN-coated gold NPs. CALNN is a 5 amino-acid long peptide.

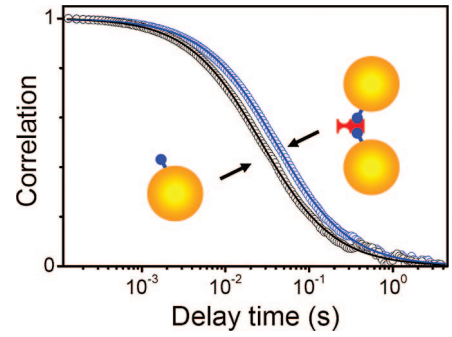

Figure 5. PhACS correlation curves obtained from 10 nm biotin monofunctionnalized NPs alone (left) and upon mixture with streptavidin (right). Solid lines represent theoretical fits using eq 2. The diffusion time increased by a factor of 1.4 upon addition of streptavidin, suggesting the formation of dumbbells (see text).

knowledge of the solution viscosity. Using these standards, we could determine *d* for different ligand-NP complexes consisting of commercial samples of 5 or 10 nm gold NPs conjugated with Goat Anti-Mouse IgG antibodies or Goat Anti-Mouse Fab'2 fragments. Interestingly the full IgG-NP complexes displayed mean hydrodynamic diameters of 10.1 ± 0.4 nm for 5 nm gold NPs and 15.5 ± 0.6 nm for 10 nm NPs, whereas for Fab-NP complexes we found 9.4 ± 0.4 and 12.5 ± 0.5 nm for 5 and 10 nm NPs, respectively. By comparing these values to the protein sizes, namely about 14 × 14 × 5 nm^3 for an IgG and 7 × 5 × 5 nm^3 for a Fab'2 fragment (see methods), one can roughly estimate the NPs coverage by the ligands as one, at most, for IgGs and one or more for Fab'2 fragments.

Recently, new NP functionalization strategies which aim at reducing the size of the ligand have emerged. For instance, thin peptide shells consisting of 5 amino-acids, (CALNN) were used to coat 7.5 nm gold NPs.[31] Using PhACS we found that *d* increased from 7.4 ± 0.3 to 8.6 ± 0.3 nm (Figure 4) upon coating the NPs. This increase of only 1.2 nm matches the estimated size of a CALNN peptide (~0.15 nm per amino acid) indicating that these NPs are most likely covered by compact layer of the peptide oriented perpendicular to the NP surface.[31] As such, PhACS should allow characterization of peptide arrangement at the surface of the NP as a function of peptide density coverage.

DLS is also a well-known method for size measurements of nano-objects down to a few nanometers. Based on scattering, it is however limited to ultraclean scattering-free environments. To emphasize the benefits of PhACS compared to DLS in turbid samples, we performed comparative PhACS and DLS measurements on samples containing 10 nm gold nanoparticles with or without 330 nm latex particles. At a latex concentration of 10^8 nanoparticles/mL, samples are clearly white. PhACS allowed for diffusion time measurements of gold NPs regardless the presence of the latex particles. The curves in both conditions were indistinguishable giving the same characteristic time of 11 ± 0.1 ms. In contrast, hydrodynamic properties of gold NP could only be performed using DLS without the latex beads (see Supporting Information).

Binding Assay. Precise measurements of diffusion coefficients (or hydrodynamic diameters) can also be used to measure quantitative molecular interactions.[32,33] When the diffusion coefficients of the two interacting species are comparable, this task is difficult and requires very high signal-to-noise ratios.[24] In this context, PhACS should be highly beneficial. To demonstrate this potential, we designed a binding assay that uses biotin and streptavidin. The biotin−streptavidin ligand−receptor system form one of the strongest noncovalent interactions with a dissociation constant between 10^{-15} and 10^{-13} M. As such, it is a well-studied model system for ligand−receptor interactions. We used 10 nm biotin monofunctionalized NPs (mf-biotin NPs)[34] mixed with streptavidin. Mf-biotin NPs alone gave a diffusion time of t_{biot} = 28.2 ± 0.2 ms. By increasing the concentration of streptavidin, the diffusion time increased to 39.9 ± 0.2 ms ≈ 1.4 × t_{biot}, a factor predicted for dumbbells,[35] indicating that streptavidin binding produced mainly dimers of mf-biotin NPs (Figure 5). Interestingly, the diffusion time decreased in excess of streptavidin (29.2 ± 0.2 ms), suggesting that binding of an isolated streptavidin on each mf-biotin NPs prevents the efficient formation of dimers.

CONCLUSION

In this paper, we introduce a new correlation method which allows quantitative determinations of the diffusion constant of absorbing nanoparticles. PhACS can be used to measure the hydrodynamic diameter of functionalized nanoparticles complexes with nanometer precisions. PhACS is also applicable to a variety of absorbing nano-objects such as silver nanoparticles, semiconductor nanocrystals,[36] or single-wall carbon nanotubes.[37] Moreover, using polarized excitation, rotational diffusion could be detected and give access to the aspect ratio of elongated objects.[38] Finally, PhACS

is not sensitive to any scattering background and should find numerous applications in live cell studies by giving access to long time scales that are not accessible for standard FCS experiments.

MATERIALS AND METHODS

Sample Prepartion. We used well-characterized gold colloids of different sizes measured by electron microscopy ($d = 4.8 \pm 1.0$, 9.2 ± 1.1, and 20.2 ± 1.3 nm), purchased from Sigma. A small volume of gold NP stock solutions (Sigma, St Louis, MO) was added into water/glycerin solutions (0%, 60%, 80%, 95% glycerin w/w) at a final concentration of about 10^{11} particles/mL ($\sim$15 nM for 10 nm gold NPs). The viscosity of each solution was measured on a rheometer maintained at constant temperature to avoid viscosity fluctuations. The samples consisted of 50 μL solutions sandwiched between two glass coverslips.

DLS measurements were performed on a Zetasizer Nano ZS. For these experiments we used pure water with 10^{11} gold NPs/mL and either none or $\sim 10^{10}$ particles/mL for latex beads. PhACS experiments were performed using the same concentrations in 80% glycerin solutions.

PhACS Optical Setup. The microscopy setup is adapted from a "photothermal heterodyne imaging" setup[17] working in the forward direction.[23] A nonresonant probe beam (HeNe, 632.8 nm) and an absorbed heating beam (532 nm, frequency doubled Nd:YAG laser) are overlaid and focused on the sample by means of a high NA microscope objective (100$\times$, NA = 1.4). The intensity of the heating beam ($\sim$100 kW/cm^2) is modulated at a frequency Ω (typically $\Omega/2\pi = 700$ kHz) by an acousto-optic modulator. The interfering probe-transmitted and forward-scattered fields are efficiently collected using a second microscope objective (80$\times$, NA = 0.8) on a fast photodiode and fed into a lock-in amplifier in order to extract the beatnote signal at Ω.[23] Photothermal images are obtained by raster scanning of the samples by means of a piezoscanner stage, whereas for PhACS the stage was kept at a fixed position. Photothermal signals are first sent to a voltage-frequency converter and then to an autocorrelator (ALV 5000).

Data Analysis. Each PhACS curve was fitted according to eq 2 with two free parameters (N and τ_D) and one known parameter (A). Standard errors are defined from the distribution of the fitted data obtained from repetitive correlation functions.

The sizes of proteins have been estimated using Swiss PDB Viewer software and a IgG2a monoclonal antibody structure as an input.[39]

Acknowledgment. We thank Jonah Shaver for careful reading of the manuscript. This research was funded by the Human Frontiers Science Program, the Région Aquitaine, and the Agence Nationale pour la Recherche (ANR).

Supporting Information Available: Figure S1: Comparative DLS and PhACS measurements. This material is available free of charge *via* the Internet at http://pubs.acs.org.

REFERENCES AND NOTES

1. Magde, D.; Elson, E.; Webb, W. W. Thermodynamic Fluctuations in a Reacting System—Measurement by Fluorescence Correlation Spectroscopy. *Phys. Rev. Lett.* **1972**, *29*, 705–708.
2. Ehrenber, M.; Rigler, R. Rotational Brownian-Motion And Fluorescence Intensity Fluctuations. *Chem. Phys.* **1974**, *4*, 390–401.
3. Aragon, S. R.; Pecora, R. Fluorescence Correlation Spectroscopy as a Probe of Molecular Dynamics. *J. Chem. Phys.* **1976**, *64*, 1791–1803.
4. Koppel, D. E.; Axelrod, D.; Schlessinger, J.; Elson, E. L.; Webb, W. W. Dynamics of Fluorescence Marker Concentration as a Probe of Mobility. *Biophys. J.* **1976**, *16*, 1315–1329.
5. Wawrezinieck, L.; Rigneault, H.; Marguet, D.; Lenne, P.-F. Fluorescence Correlation Spectroscopy Diffusion Laws to Probe the Submicron Cell Membrane Organization. *Biophys. J.* **2005**, *89*, 4029–4042.
6. Schwille, P.; Haupts, U.; Maiti, S.; Webb, W. W. Molecular Dynamics in Living Cells Observed by Fluorescence Correlation Spectroscopy with One- and Two-Photon Excitation. *Biophys. J.* **1999**, *77*, 2251–2265.
7. Schwille, P.; Kummer, S.; Heikal, A. A.; Moerner, W. E.; Webb, W. W. Fluorescence Correlation Spectroscopy Reveals Fast Optical Excitation-Driven Intramolecular Dynamics of Yellow Fluorescent Proteins. *Proc. Natl. Acad. Sci. U.S.A.* **2000**, *97*, 151–156.
8. Wang, Z.; Shah, J. V.; Berns, M. W.; Cleveland, D. W. *In Vivo* Quantitative Studies of Dynamic Intracellular Processes Using Fluorescence Correlation Spectroscopy. *Biophys. J.* **2006**, *91*, 343–351.
9. Bacia, K.; Kim, S. A.; Schwille, P. Fluorescence Cross-Correlation Spectroscopy in Living Cells. *Nat. Methods* **2006**, *3*, 83–89.
10. Ries, J.; Schwille, P. Studying Slow Membrane Dynamics with Continuous Wave Scanning Fluorescence Correlation Spectroscopy. *Biophys. J.* **2006**, *91*, 1915–1924.
11. Connor, E. E.; Mwamuka, J.; A., G.; C. J., M.; M. D., W. Gold Nanoparticles are Taken Up by Human Cells but Do Not Cause Acute Cytotoxicity. *Small* **2005**, *1*, 325–327.
12. Gannon, C.; Patra, C.; Bhattacharya, R.; Mukherjee, P.; Curley, S. Intracellular Gold Nanoparticles Enhance Non-Invasive Radiofrequency Thermal Destruction of Human Gastrointestinal Cancer Cells. *J. Nanobiotechnol.* **2008**, *6*, 2-1–2-9.
13. Yguerabide, J.; Yguerabide, E. E. Light-Scattering Submicroscopic Particles as Highly Fluorescent Analogs and their Use as Tracer Labels in Clinical and Biological Applications. *Anal. Biochem.* **1998**, *262*, 137–156.
14. Dubin, S. B.; Lunacek, J. H.; Benedek, G. B. Observation of the Spectrum of Light Scattered by Solutions of Biological Macromolecules. *Proc. Natl. Acad. Sci. U.S.A.* **1967**, *57*, 1164–1171.
15. Berne, B. J.; Pecora, R. *Dynamic Light Scattering with Applications to Chemistry, Biology and Physics*; John Wiley and Sons: New-York, 1976; pp 144−149.
16. Boyer, D.; Tamarat, P.; Maali, A.; Lounis, B.; Orrit, M. Photothermal Imaging of Nanometer-Sized Metal Particles Among Scatterers. *Science* **2002**, *297*, 1160–1163.
17. Berciaud, S.; Cognet, L.; Blab, G. A.; Lounis, B. Photothermal Heterodyne Imaging of Individual Nonfluorescent Nanoclusters and Nanocrystals. *Phys. Rev. Lett.* **2004**, *93*, 257402-1–257402-4.
18. Lindfors, K.; Kalkbrenner, T.; Stoller, P.; Sandoghdar, V. Detection and Spectroscopy of Gold Nanoparticles Using Supercontinuum White Light Confocal Microscopy. *Phys. Rev. Lett.* **2004**, *93*, 037401-1–037401-4.
19. Arbouet, A.; Christofilos, D.; Del Fatti, N.; Vallee, F.; Huntzinger, J. R.; Arnaud, L.; Billaud, P.; Broyer, M. Direct Measurement of the Single-Metal-Cluster Optical Absorption. *Phys. Rev. Lett.* **2004**, *93*, 127401-1–127401-4.
20. Ignatovich, F. V.; Novotny, L. Real-Time and Background-Free Detection of Nanoscale Particles. *Phys. Rev. Lett.* **2006**, *96*, 013901-1–013901-4.
21. Van Dijk, M. A.; Tchebotareva, A. L.; Orrit, M.; Lippitz, M.; Berciaud, S.; Lasne, D.; Cognet, L.; Lounis, B. Absorption and Scattering Microscopy of Single Metal Nanoparticles. *Phys. Chem. Chem. Phys.* **2006**, *8*, 3486–3695.
22. Lasne, D.; Blab, G. A.; Berciaud, S.; Heine, M.; Groc, L.; Choquet, D.; Cognet, L.; Lounis, B. Single Nanoparticle Photothermal Tracking (SNaPT) of 5-nm Gold Beads in Live Cells. *Biophys. J.* **2006**, *91*, 4598–4604.

23. Berciaud, S.; Lasne, D.; Blab, G. A.; Cognet, L.; Lounis, B. Photothermal Heterodyne Imaging of Individual Metallic Nanoparticles: Theory *versus* Experiments. *Phys. Rev. B* **2006**, *73*, 045424-1–045424-8.
24. Meseth, U.; Wohland, T.; Rigler, R.; Vogel, H. Resolution of Fluorescence Correlation Measurements. *Biophys. J.* **1999**, *76*, 1619–1631.
25. Enderlein, J.; Gregor, I.; Patra, D.; Fitter, J. Art and Artefacts of Fluorescence Correlation Spectroscopy. *Curr. Pharm. Biotechnol.* **2004**, *5*, 155–161.
26. Widengren, J.; Mets, U.; Rigler, R. Fluorescence Correlation Spectroscopy of Triplet States in Solution: A Theoretical and Experimental Study. *J. Phys. Chem.* **1995**, *99*, 13368–13379.
27. Davis, L. M.; Shen, G. Q. Accounting for Triplet and Saturation Effects in FCS Measurements. *Curr. Pharm. Biotechnol.* **2006**, *7*, 287–301.
28. Link, S.; El-Sayed, M. A. Optical Properties and Ultrafast Dynamics of Metallic Nanocrystals. *Annu. Rev. Phys. Chem.* **2003**, *54*, 331–366.
29. Enderlein, J.; Gregor, I.; Patra, D.; Dertinger, T.; Kaupp, U. B. Performance of Fluorescence Correlation Spectroscopy for Measuring Diffusion and Concentration. *Chemphyschem* **2005**, *6*, 2324–2336.
30. Groc, L.; Lafourcade, M.; Heine, M.; Renner, M.; Racine, V.; Sibarita, J. B.; Lounis, B.; Choquet, D.; Cognet, L. Surface Trafficking of Neurotransmitter Receptor: Comparison between Single-Molecule/Quantum Dot Strategies. *J. Neurosci.* **2007**, *27*, 12433–12437.
31. Levy, R.; Thanh, N. T.; Doty, R. C.; Hussain, I.; Nichols, R. J.; Schiffrin, D. J.; Brust, M.; Fernig, D. G. Rational and Combinatorial Design of Peptide Capping Ligands for Gold Nanoparticles. *J. Am. Chem. Soc.* **2004**, *126*, 10076–10084.
32. Kinjo, M.; Rigler, R. Ultrasensitive Hybridization Analysis Using Fluorescence Correlation Spectroscopy. *Nucleic Acids Res.* **1995**, *23*, 1795–1799.
33. Schwille, P.; Oehlenschlager, F.; Walter, N. G. Quantitative Hybridization Kinetics of DNA Probes to RNA in Solution Followed by Diffusional Fluorescence Correlation Analysis. *Biochemistry* **1996**, *35*, 10182–10193.
34. Levy, R.; Wang, Z. X.; Duchesne, L.; Doty, R. C.; Cooper, A. I.; Brust, M.; Fernig, D. G. A Generic Approach to Monofunctionalized Protein-like Gold Nanoparticles Based on Immobilized Metal Ion Affinity Chromatography. *Chembiochem* **2006**, *7*, 592–594.
35. Swanson, E.; Teller, D. C.; de Haen, C. The Low Reynolds Number Translational Friction of Ellipsoids, Cylinders, Dumbbells, and Hollow Spherical Caps. Numerical Testing of the Validity of the Modified Oseen Tensor in Computing the Friction of Objects Modeled as Beads on a Shell. *J. Chem. Phys.* **1978**, *68*, 5097–5102.
36. Berciaud, S.; Cognet, L.; Lounis, B. Photothermal Absorption Spectroscopy of Individual Semiconductor Nanocrystals. *Nano Lett.* **2005**, *5*, 2160–2163.
37. Berciaud, S.; Cognet, L.; Poulin, P.; Weisman, R. B.; Lounis, B. Absorption Spectroscopy of Individual Single-Walled Carbon Nanotubes. *Nano Lett.* **2007**, *7*, 1203–1207.
38. Tsay, J. M.; Doose, S.; Weiss, S. Rotational and Translational Diffusion of Peptide-Coated CdSe/CdS/ZnS Nanorods Studied by Fluorescence Correlation Spectroscopy. *J. Am. Chem. Soc.* **2006**, *128*, 1639–1647.
39. Harris, L. J.; Larson, S. B.; Hasel, K. W.; McPherson, A. Refined Structure of an Intact IgG2a Monoclonal Antibody. *Biochemistry* **1997**, *36*, 1581–1597.